Electronic Supporting Information

Selective inclusion of PO_4^{3-} within persistent dimeric capsules of a tris(thiourea) receptor and evidence of cation/solvent sealed unimolecular capsules

*Sandeep Kumar Dey and Gopal Das**

Department of Chemistry, Indian Institute of Technology Guwahati, Assam, 781039, India.

Fax: +91-361-258-2349; Tel: +91-361-258-2313

E-mail: gdas@iitg.ernet.in

Characterization of receptor L:

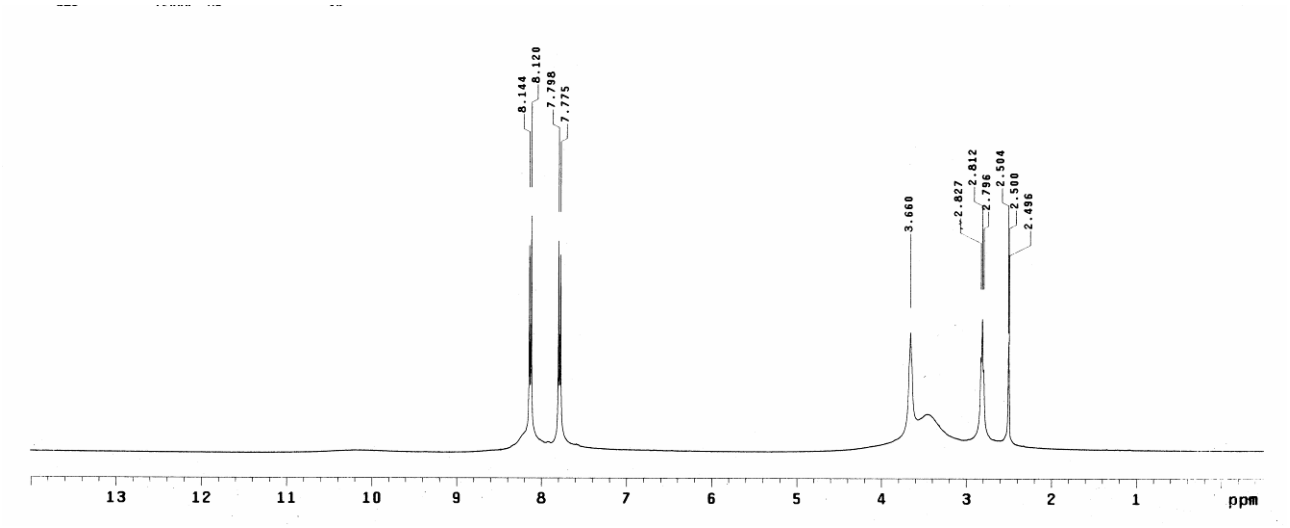

Figure S1. ^{1}H NMR spectrum of **L** in DMSO-d_6 at 298 K.

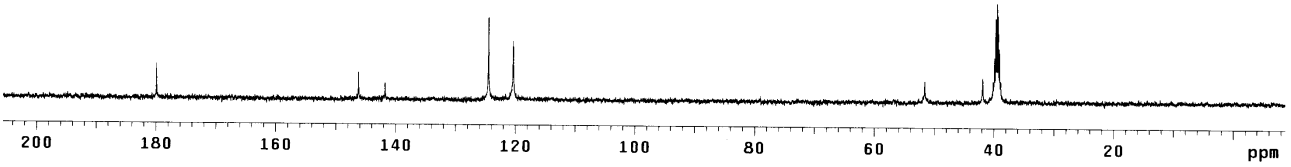

Figure S2. ^{13}C NMR spectrum of **L** in DMSO-d_6 at 298 K.

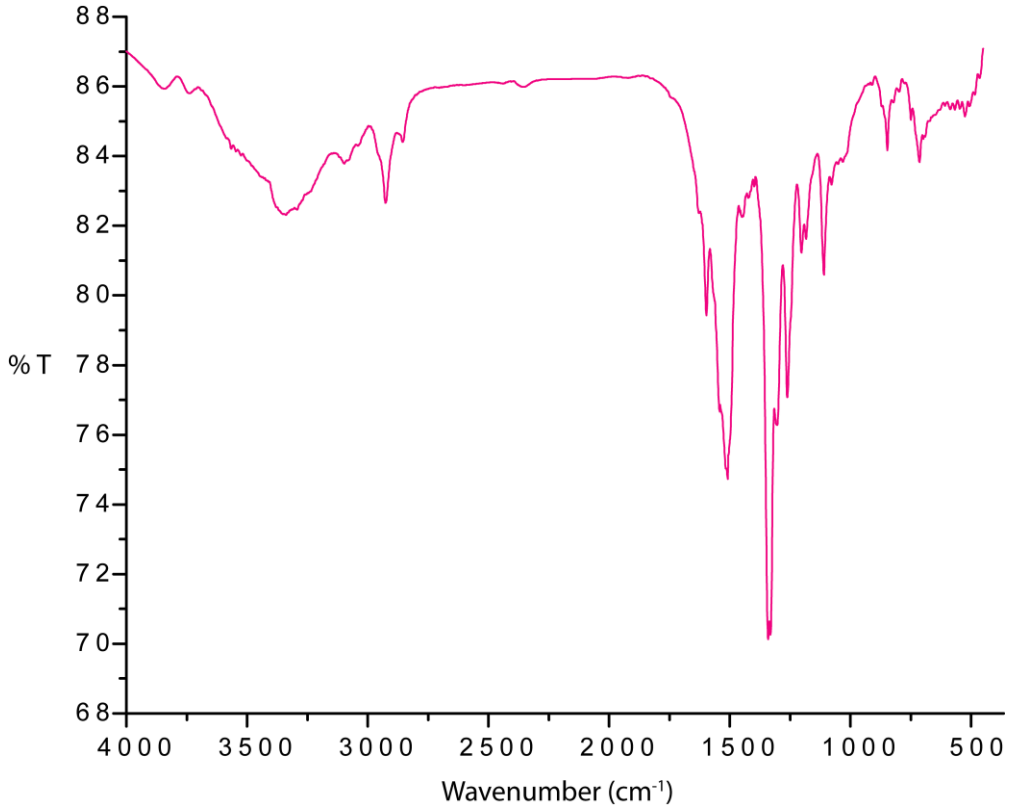

Figure S3. FT-IR spectrum of receptor **L** recorded in KBr pellet.

Characterization of HPO_4^{2-}–complex, *[2(HL)$^+$•HPO_4^{2-}]•3H_2O* (1a):

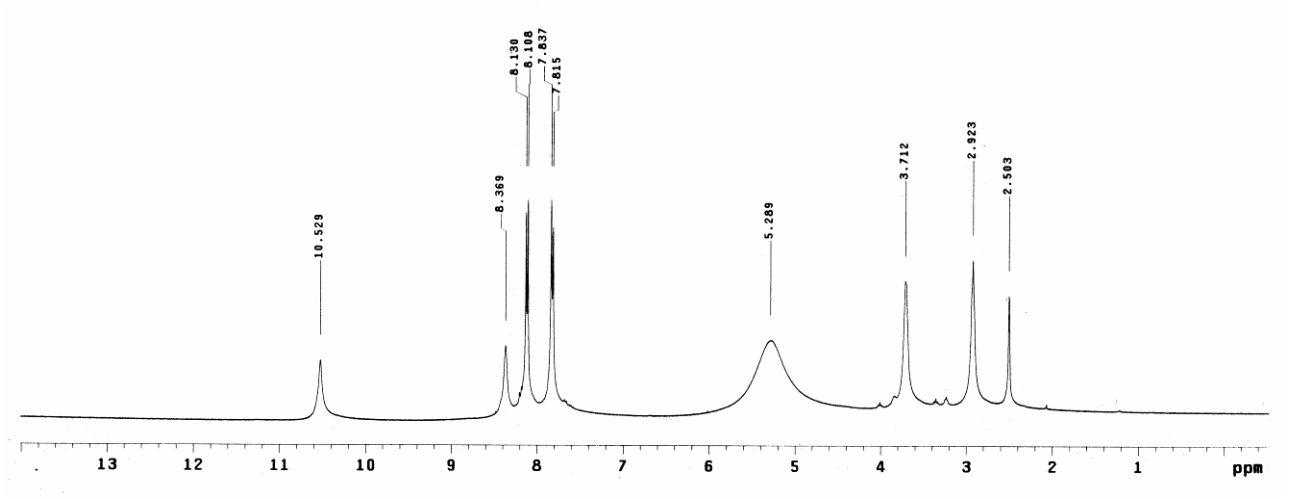

Figure S4. ^{1}H NMR spectrum of complex **1a** in DMSO-d_6 at 298 K.

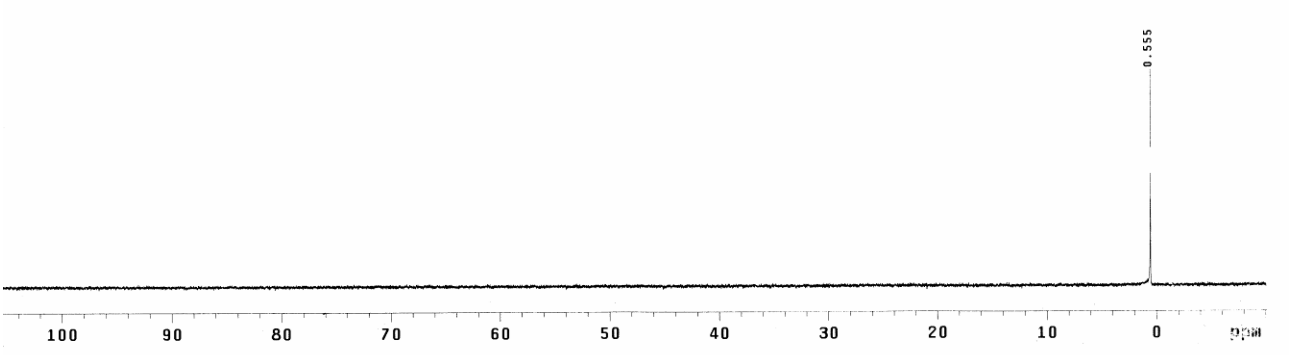

Figure S5. ^{31}P NMR spectrum of complex **1a** in DMSO-d_6 at 298 K.

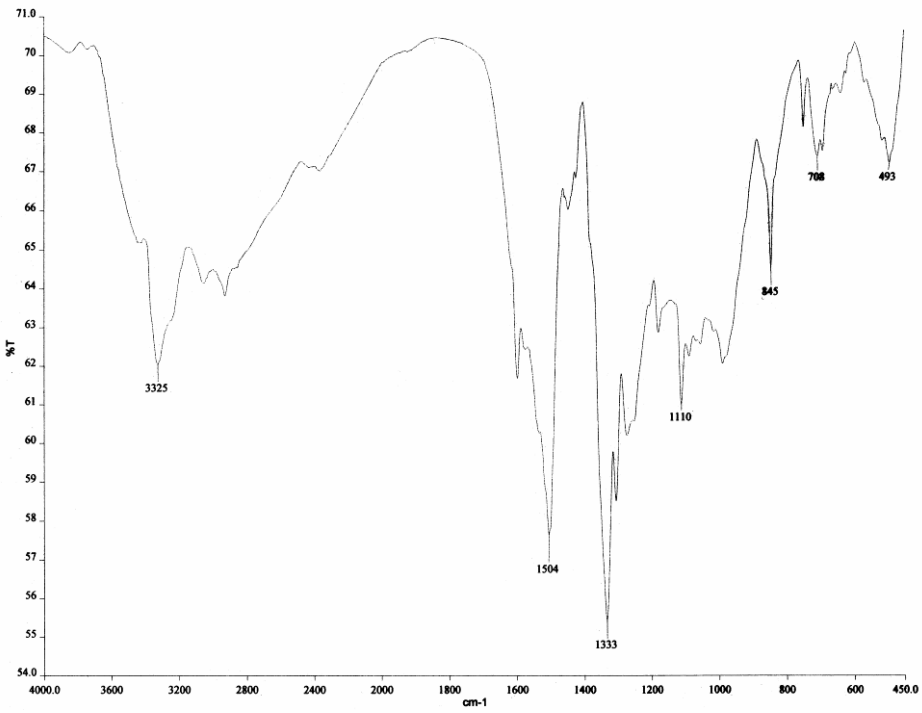

Figure S6. FT-IR spectrum of complex **1a** recorded in KBr pellet.

Characterization of PO_4^{3-}–encapsulated complex, *3TBA$^+$[2L(PO_4^{3-})]2MeCN* (1):

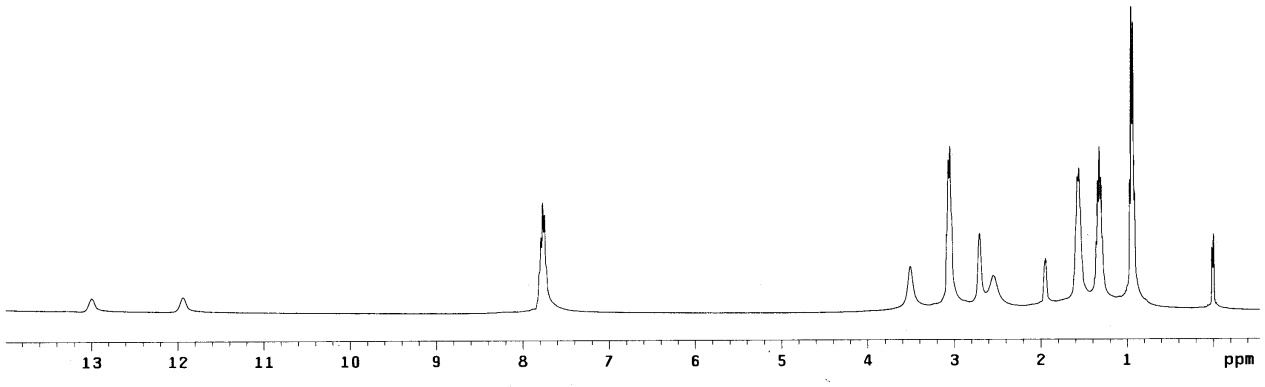

Figure S7. ^{1}H NMR spectrum of complex **1** in DMSO-d_6 at 298 K.

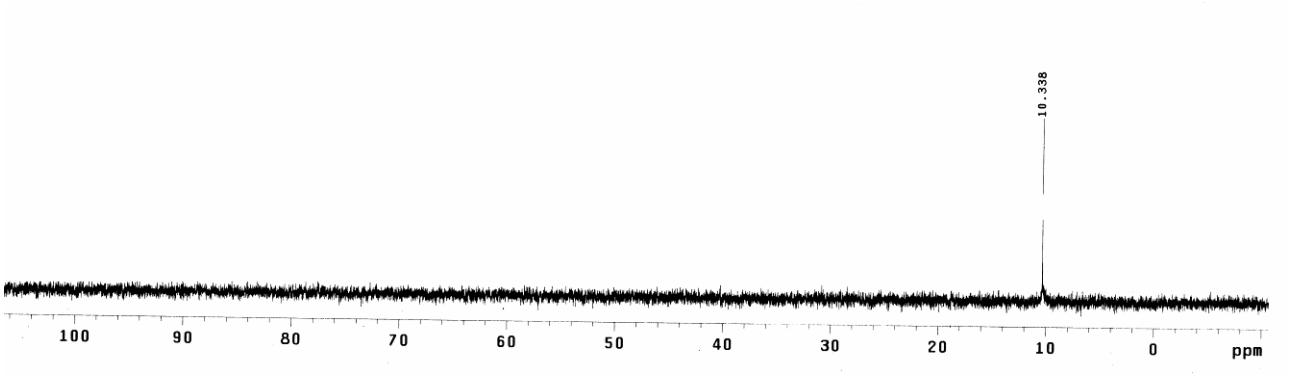

Figure S8. ^{31}P NMR spectrum of complex **1** in DMSO-d_6 at 298 K.

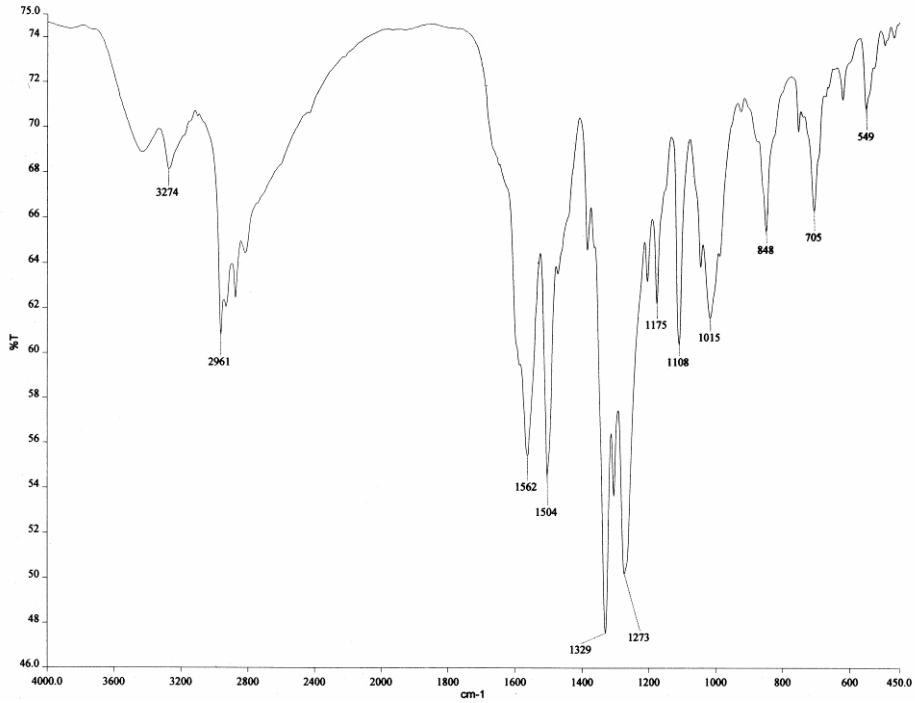

Figure S9. FT-IR spectrum of complex **1** recorded in KBr pellet.

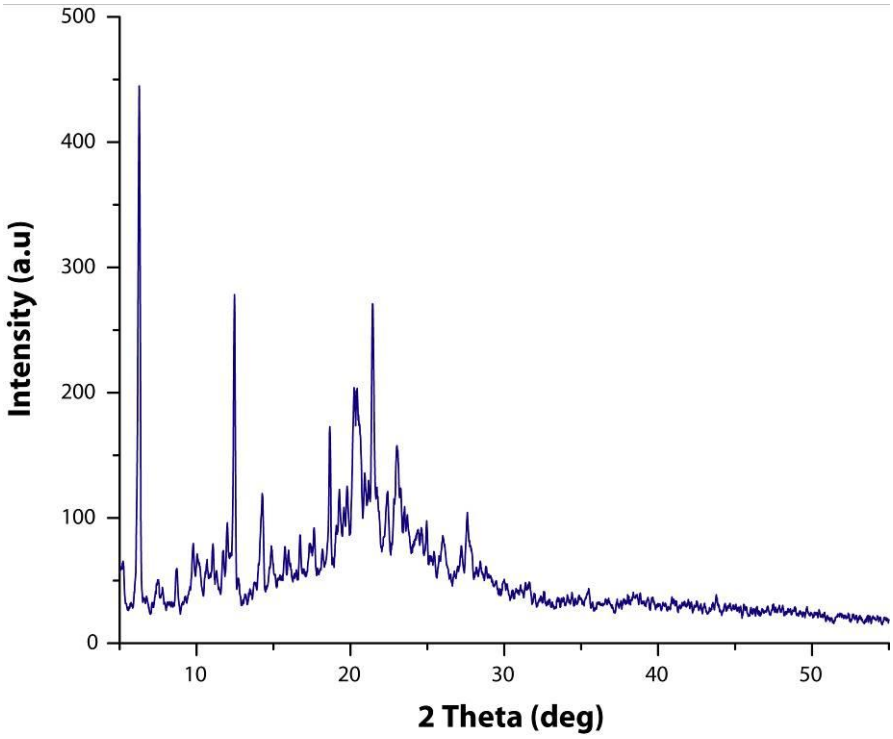

Figure S10. Powder XRD patterns of complex **1** recorded with dried crystalline powders.

Characterization of PO_4^{3-}–encapsulated complex, *3TEA⁺[2L(PO_4^{3-})]* (1b):

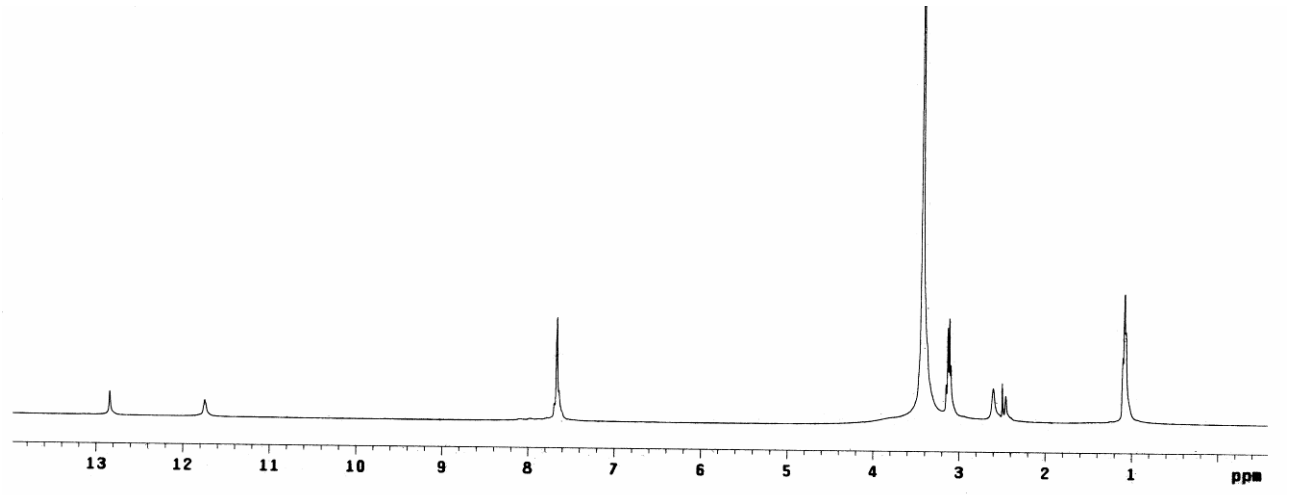

Figure S11. ^{1}H NMR spectrum of complex **1b** in DMSO-d_6 at 298 K.

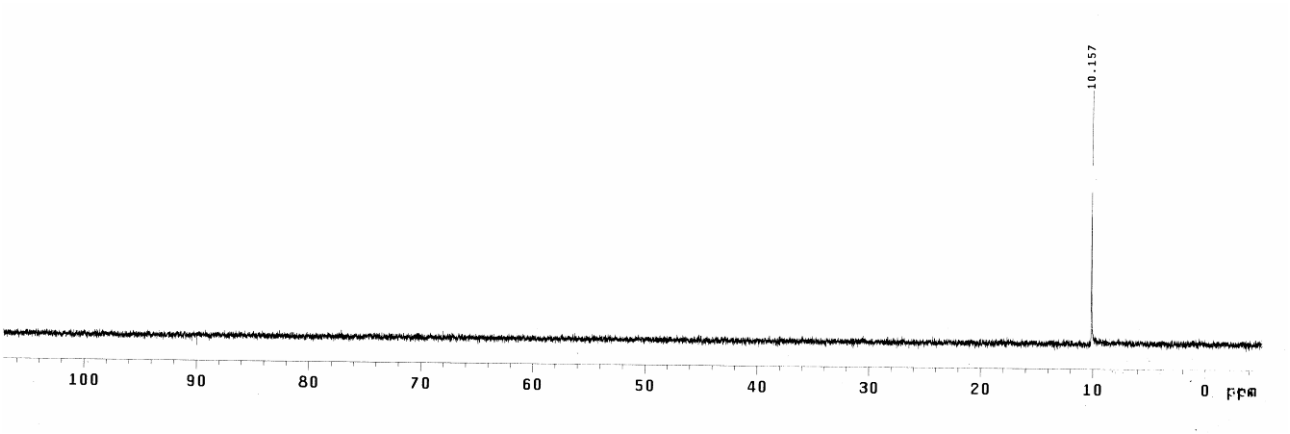

Figure S12. ^{31}P NMR spectrum of complex **1b** in DMSO-d_6 at 298 K.

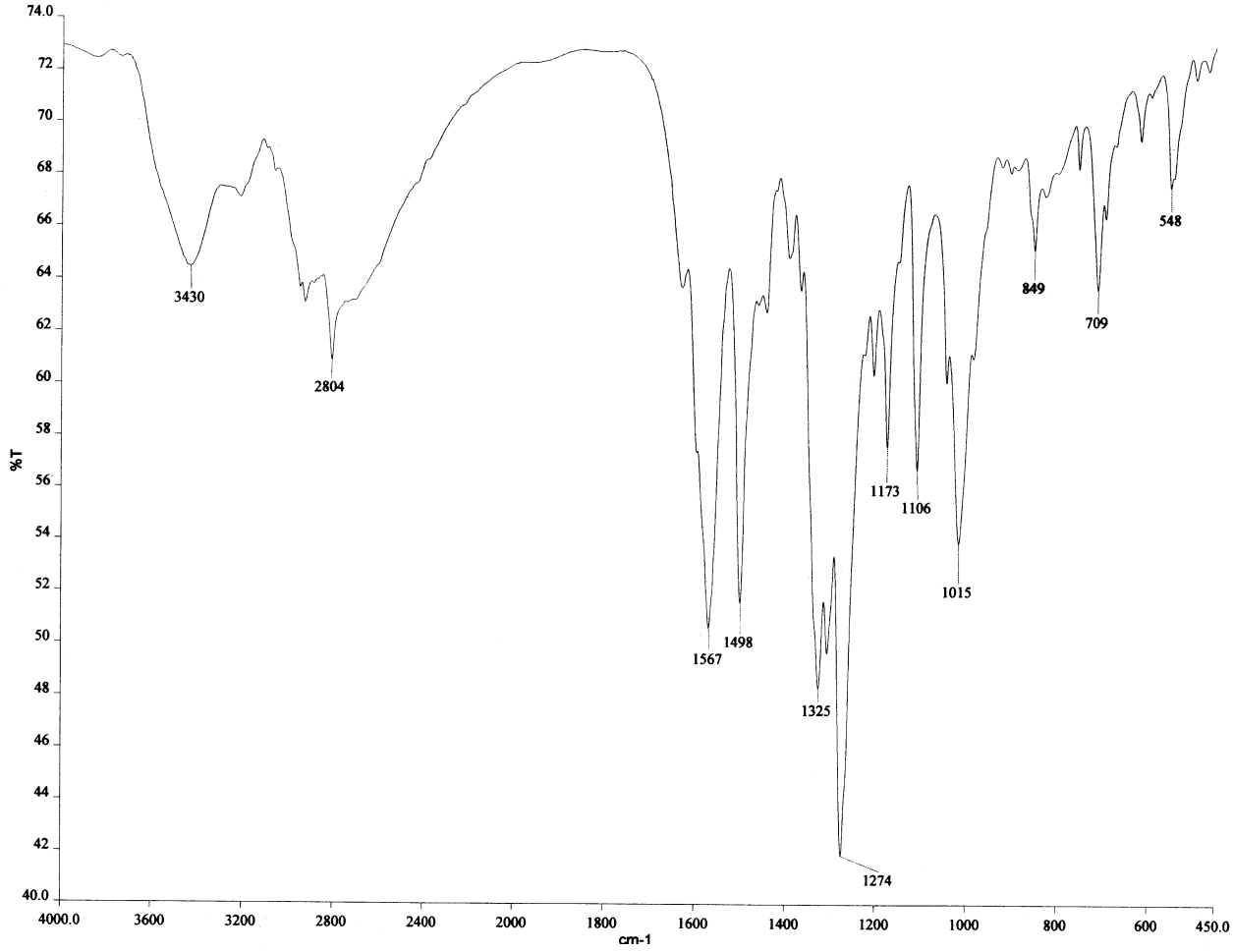

Figure S13. FT-IR spectrum of complex **1b** recorded in KBr pellet.

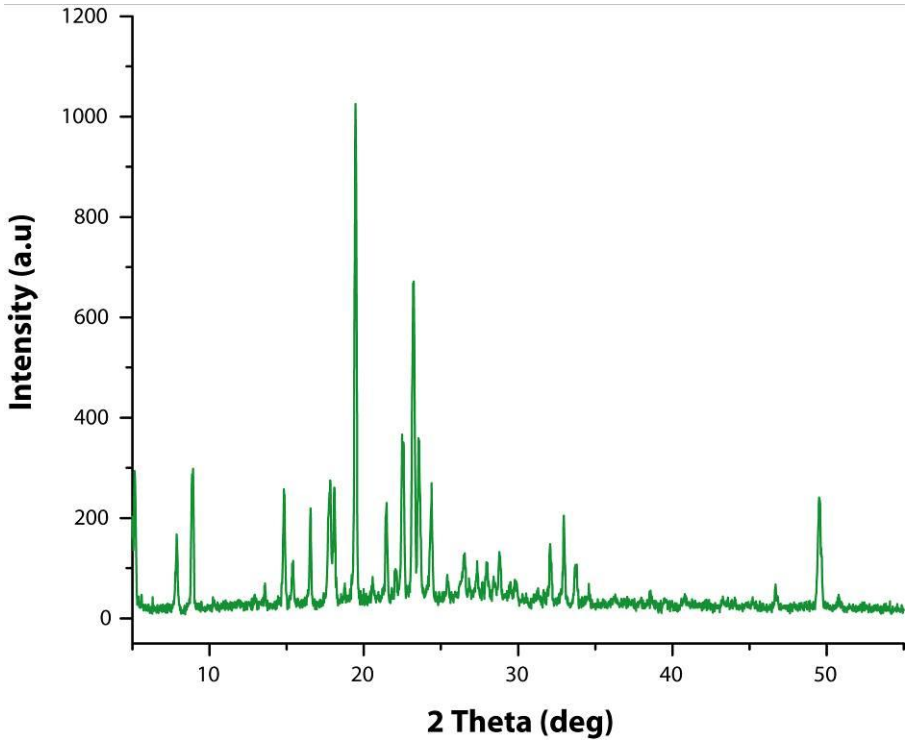

Figure S14. Powder XRD patterns of complex **1b** recorded with dried crystalline powders.

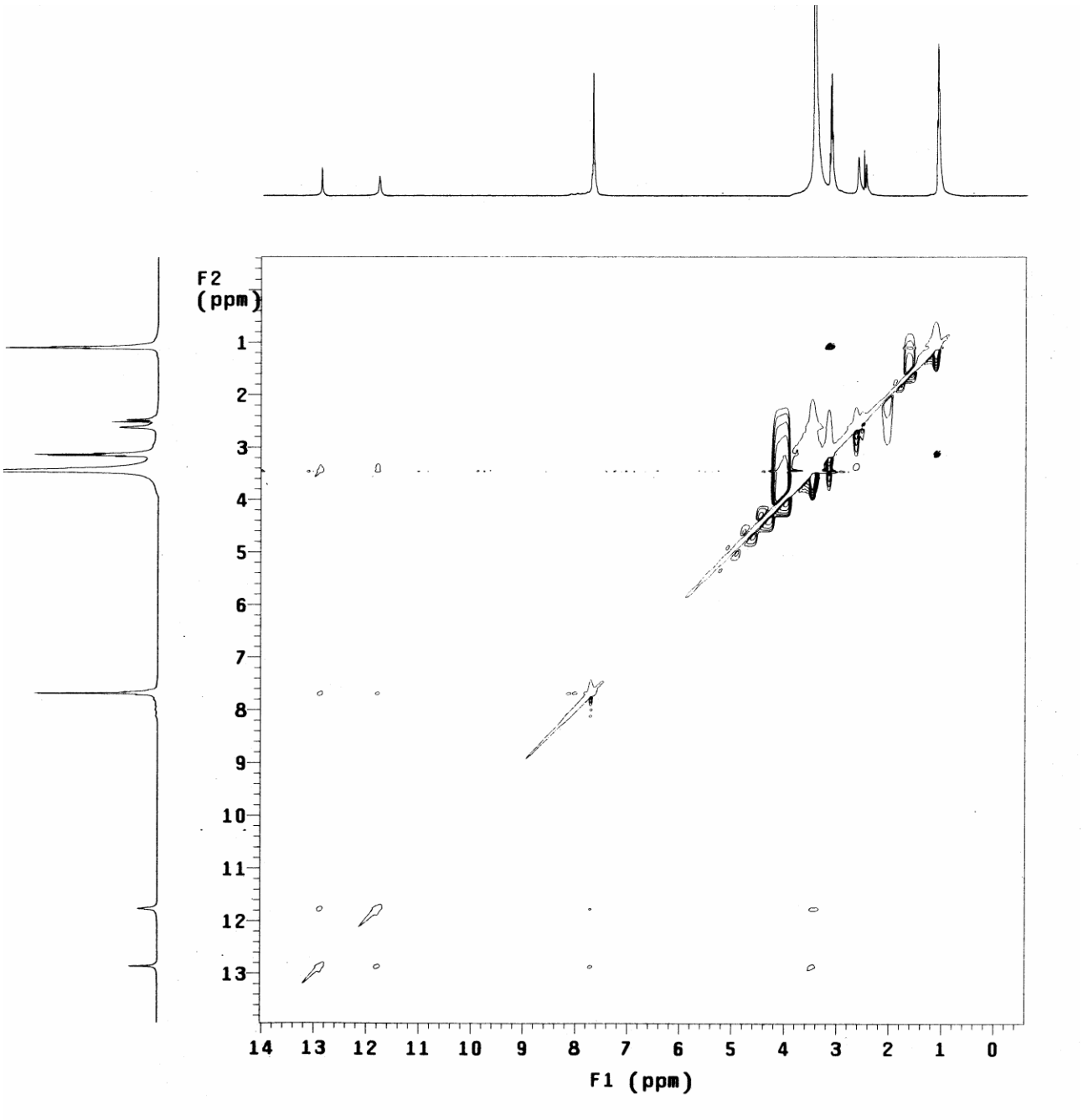

Figure S15. 2D-NOESY NMR spectrum of complex **1b** in DMSO-d_6 at 298 K.

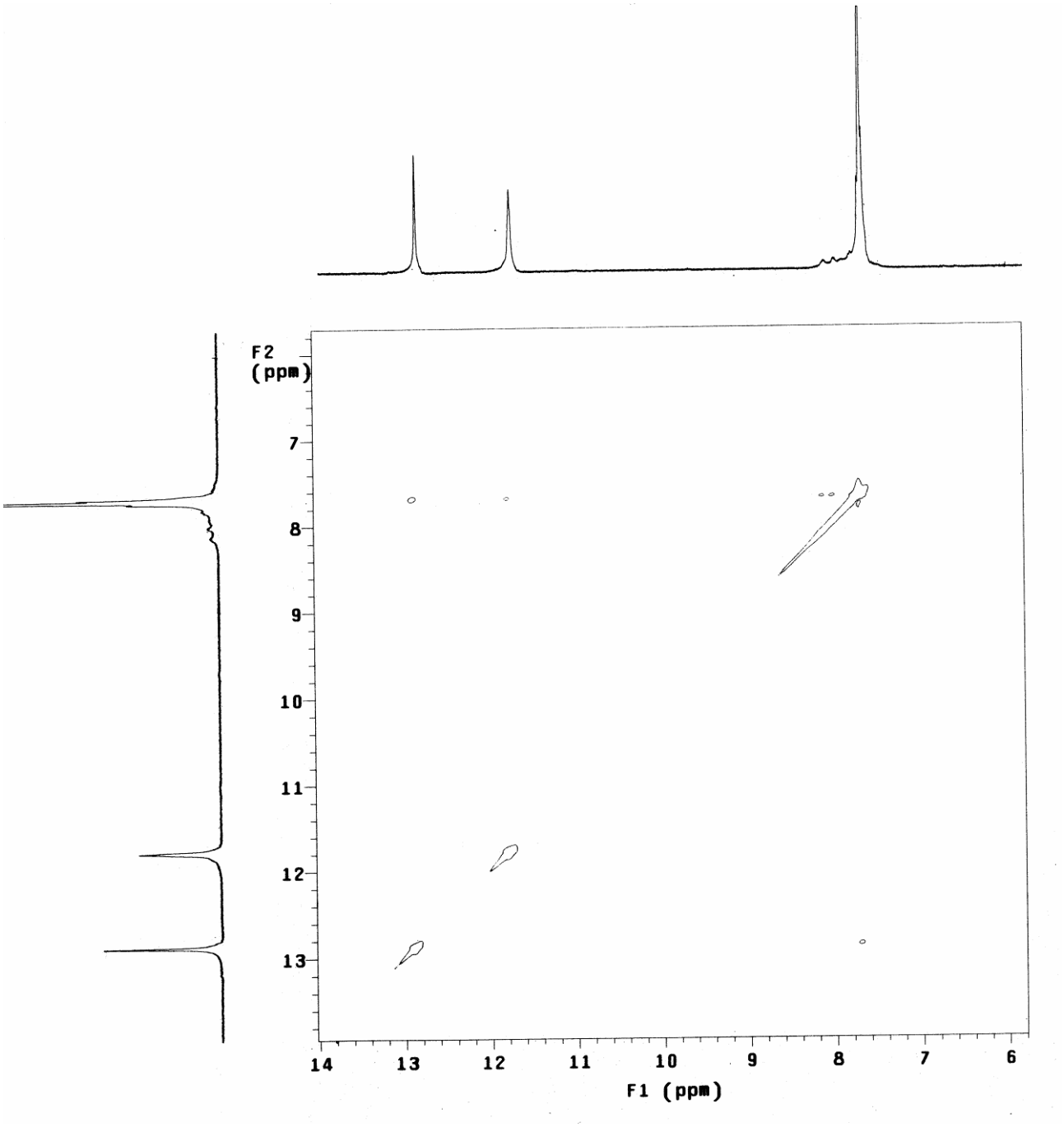

Figure S16. Partial (aromatic region) 2D-NOESY NMR spectrum of complex **1b** in DMSO-d_6 at 298 K, in presence of 0.5 equivalent 2:1 mixture of TBA(OH) and TBA(H_2PO_4).

Characterization of F^--encapsulated complex, *TBA$^+$[L(F$^-$)]•2DMSO* (2a):

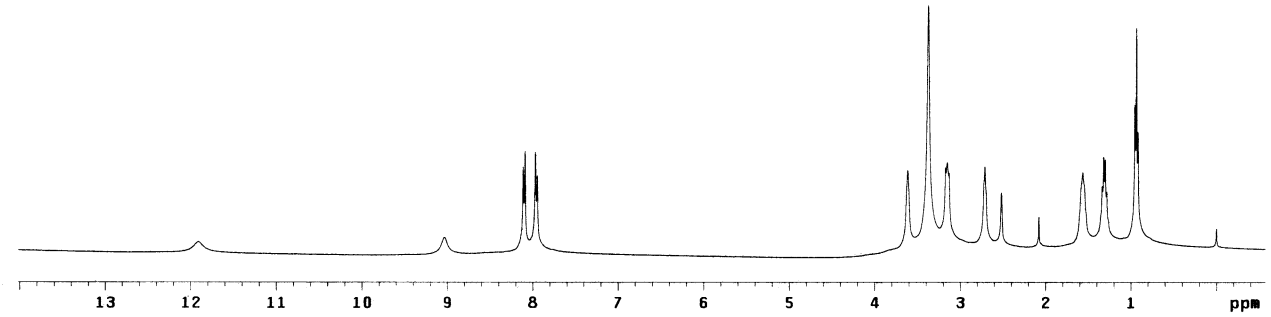

Figure S17. ^{1}H NMR spectrum of complex **2a** in DMSO-d_6 at 298 K.

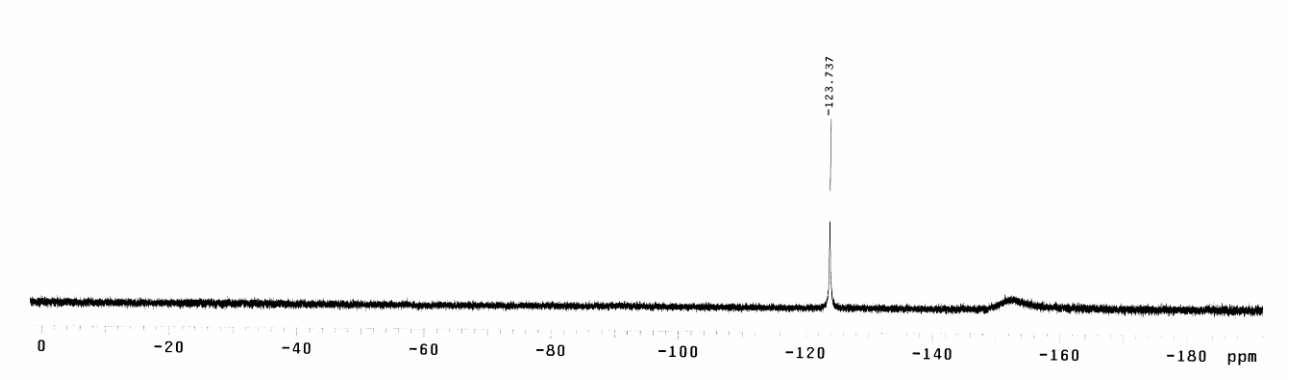

Figure S18. ^{19}F NMR spectrum of complex **2a** in DMSO-d_6 at 298 K.

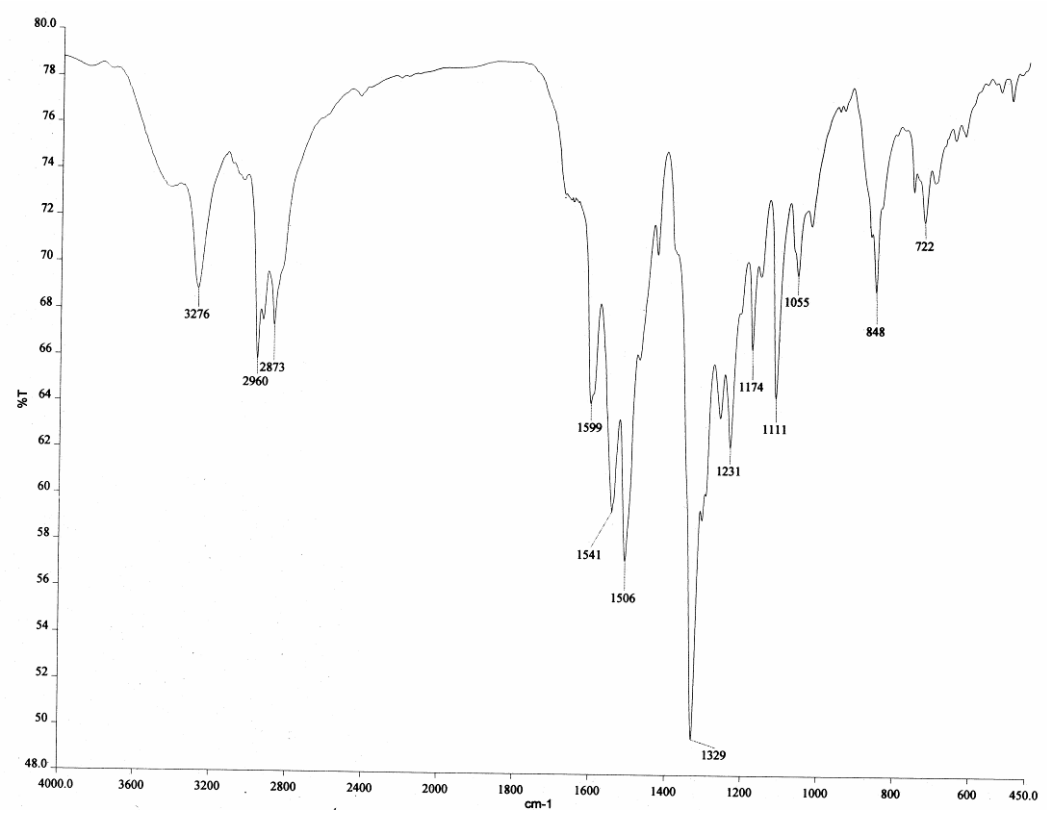

Figure S19. FT-IR spectrum of complex **2a** recorded in KBr pellet.

Characterization of CO_3^{2-}–encapsulated complex, *2TEA$^+$[2L(CO_3^{2-})]* (3):

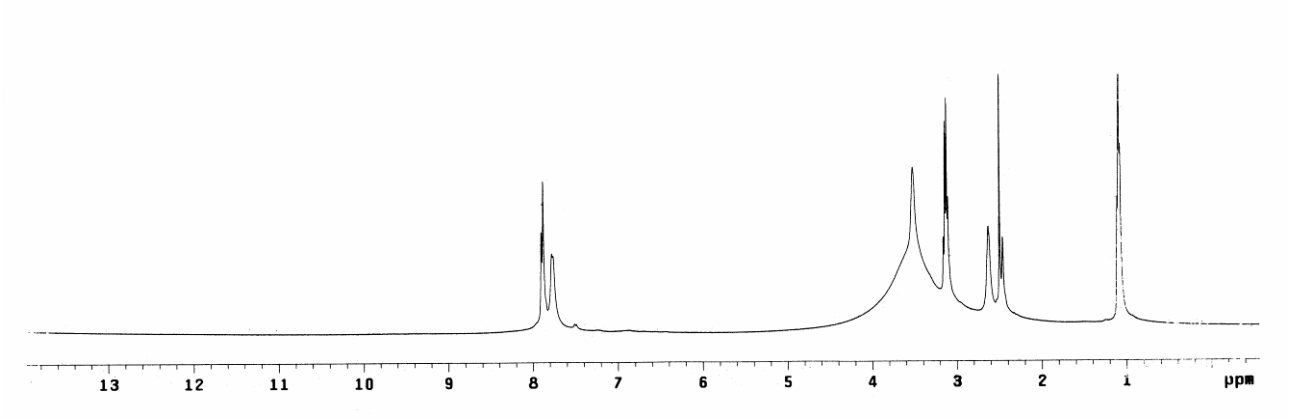

Figure S20. ^{1}H NMR spectrum of complex **3** in DMSO-d_6 at 298 K.

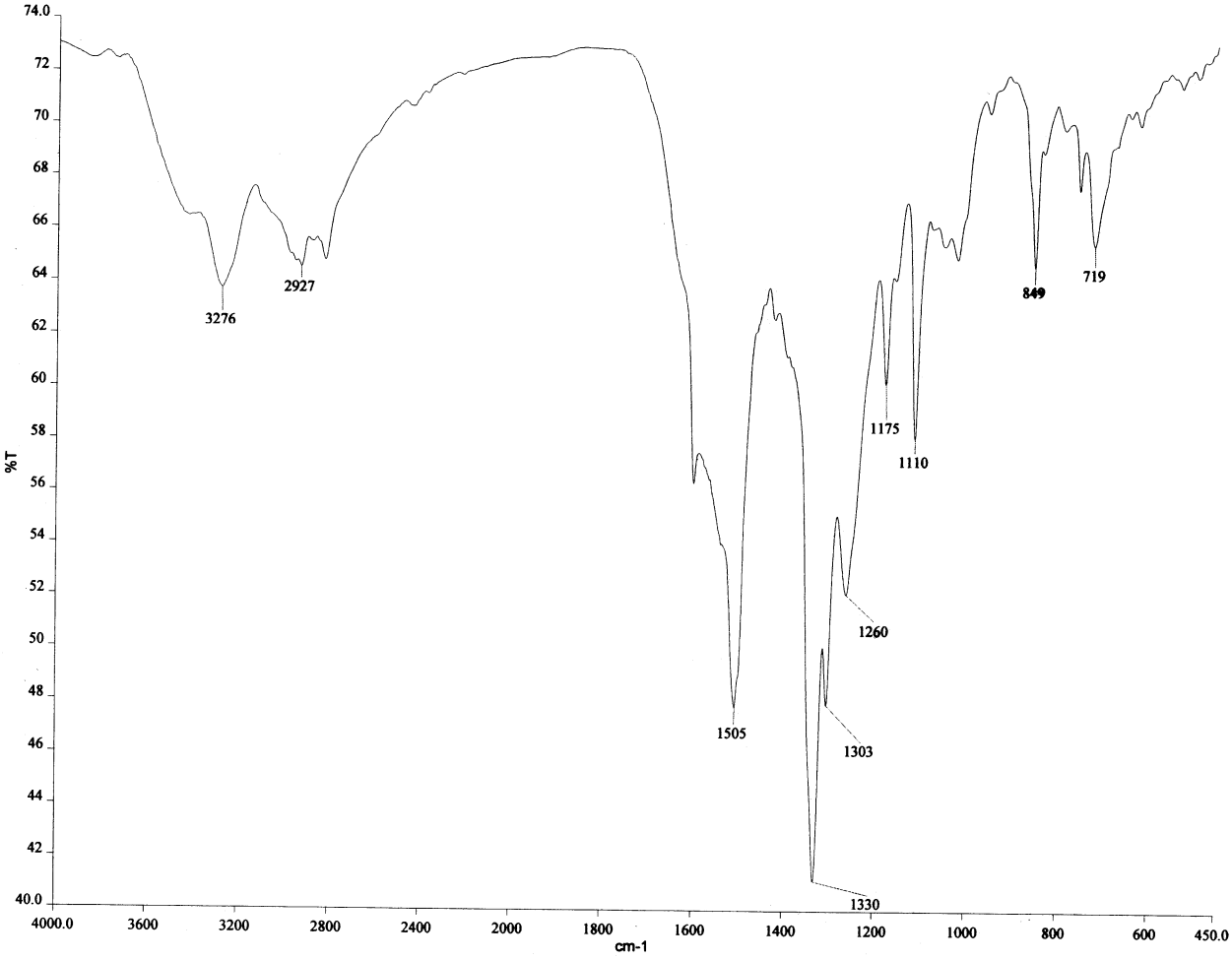

Figure S21. FT-IR spectrum of complex **3** recorded in KBr pellet.

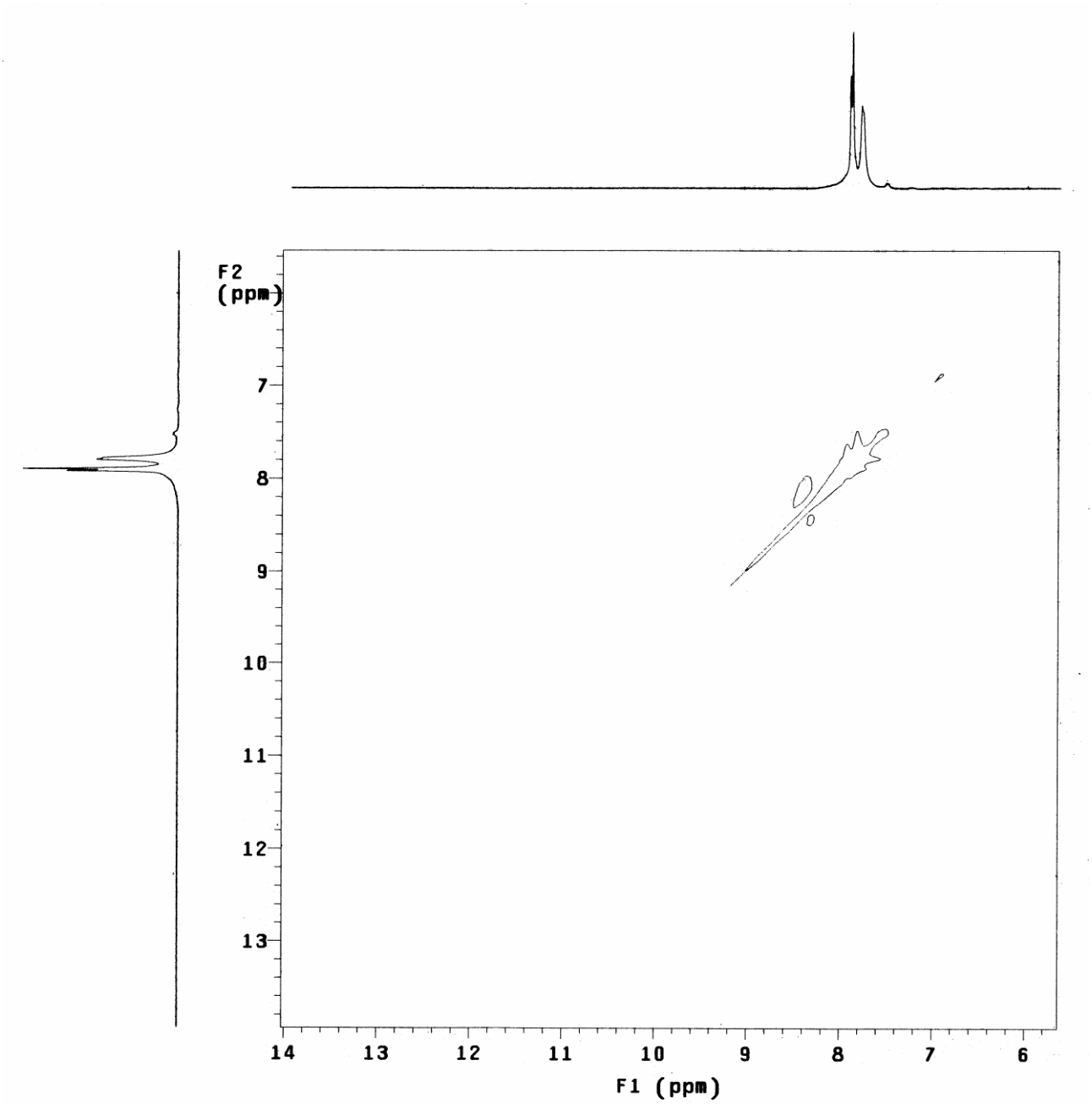

Figure S22. Partial (aromatic region) 2D-NOESY NMR spectrum of complex **3** in DMSO-d_6 at 298 K.

Characterization of SO_4^{2-}–encapsulated complex, *2TBA*$^+$*[L(SO_4^{2-})]* (4):

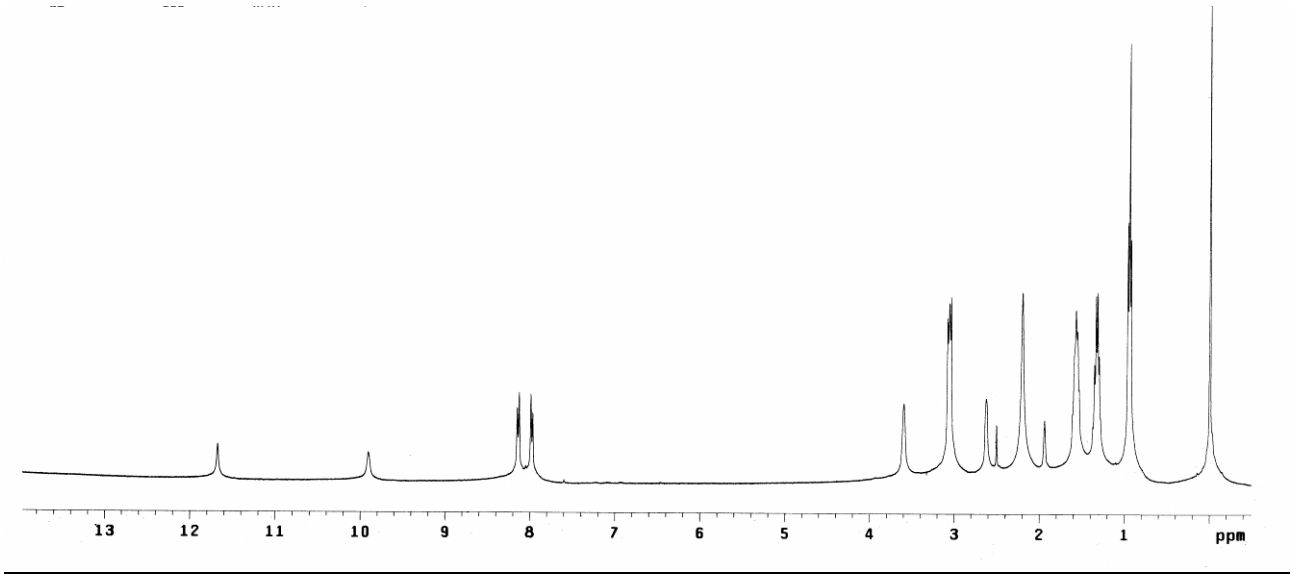

Figure S23. ^{1}H NMR spectrum of complex **4** in DMSO-d_6 at 298 K.

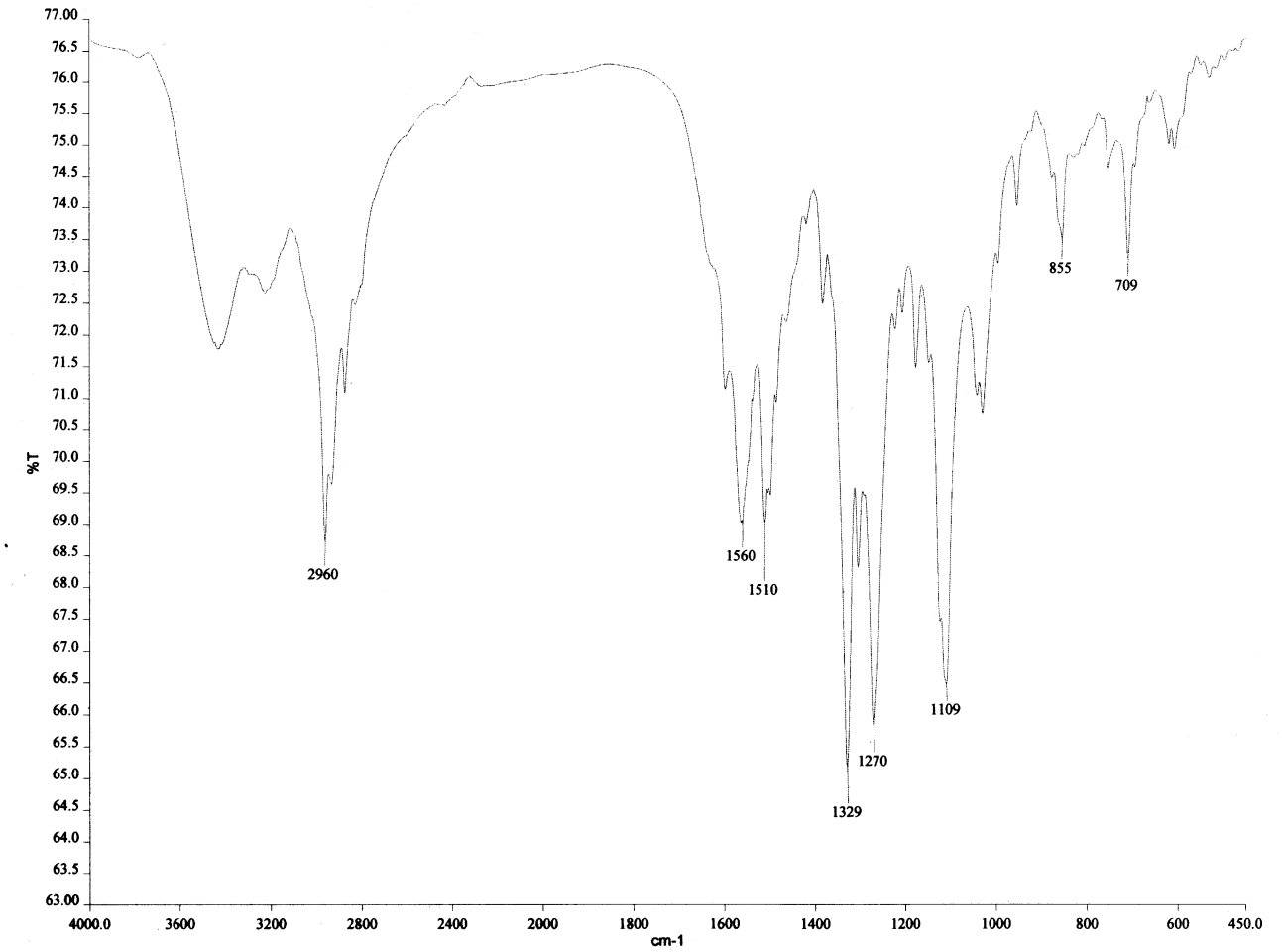

Figure S24. FT-IR spectrum of complex **4** recorded in KBr pellet.

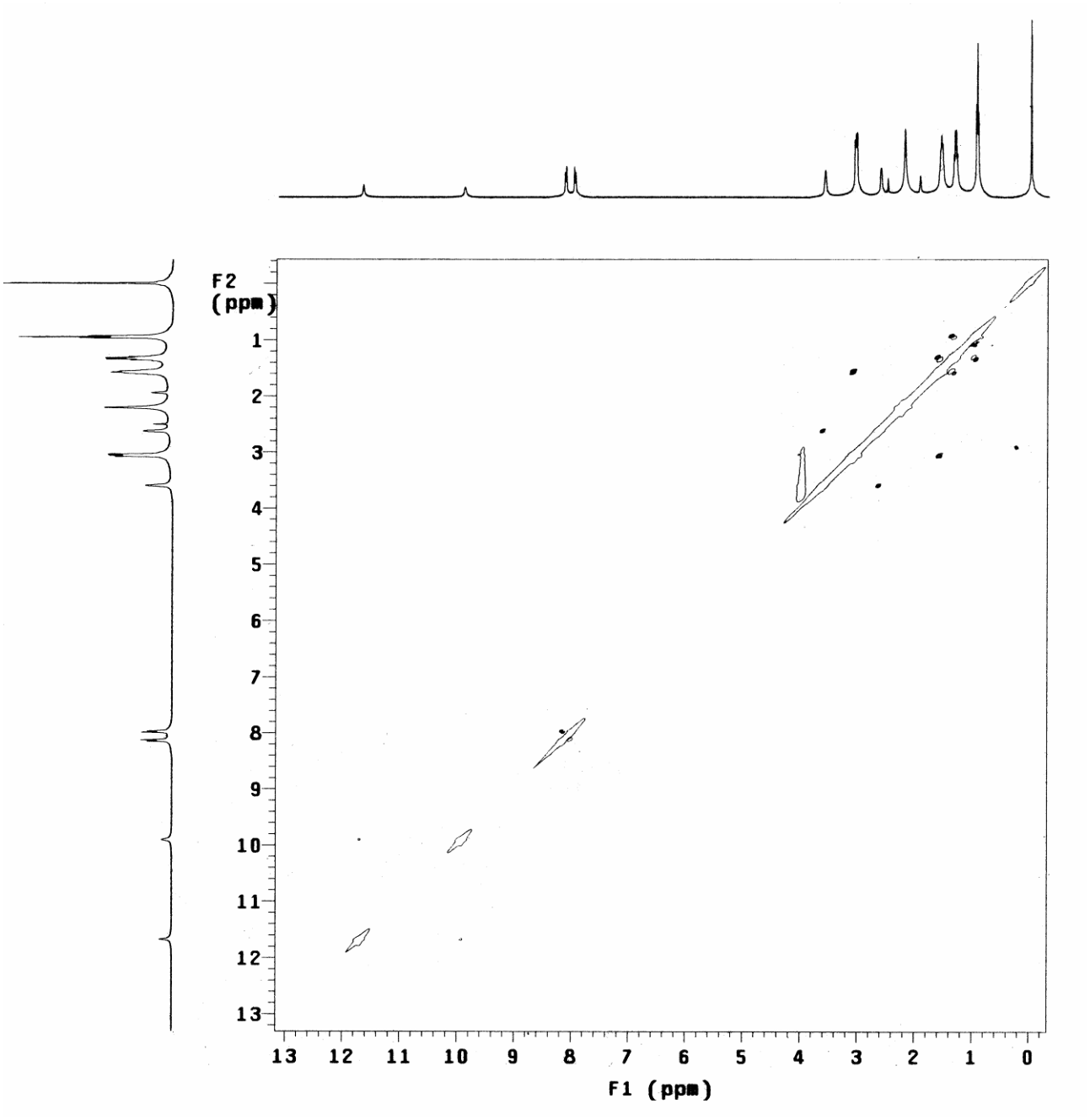

Figure S25. 2D-NOESY NMR spectrum of complex **4** in DMSO-d_6 at 298 K.

Characterization of Cl^-–complex, *[(HL)$^+$•Cl$^-$]•DMF* (5):

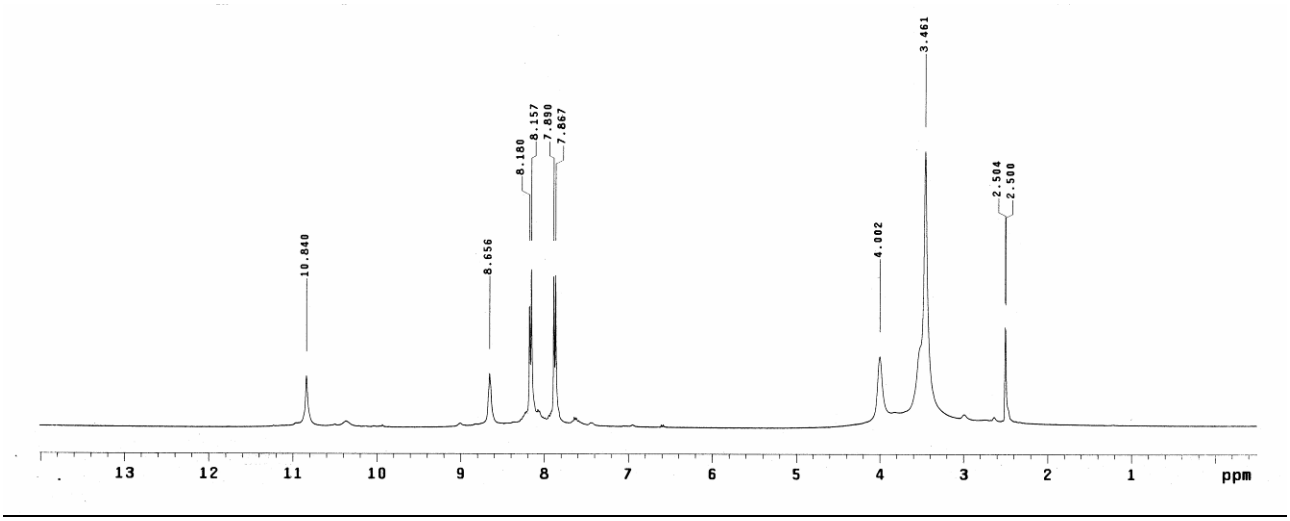

Figure S26. ^{1}H NMR spectrum of complex **5** in DMSO-d_6 at 298 K.

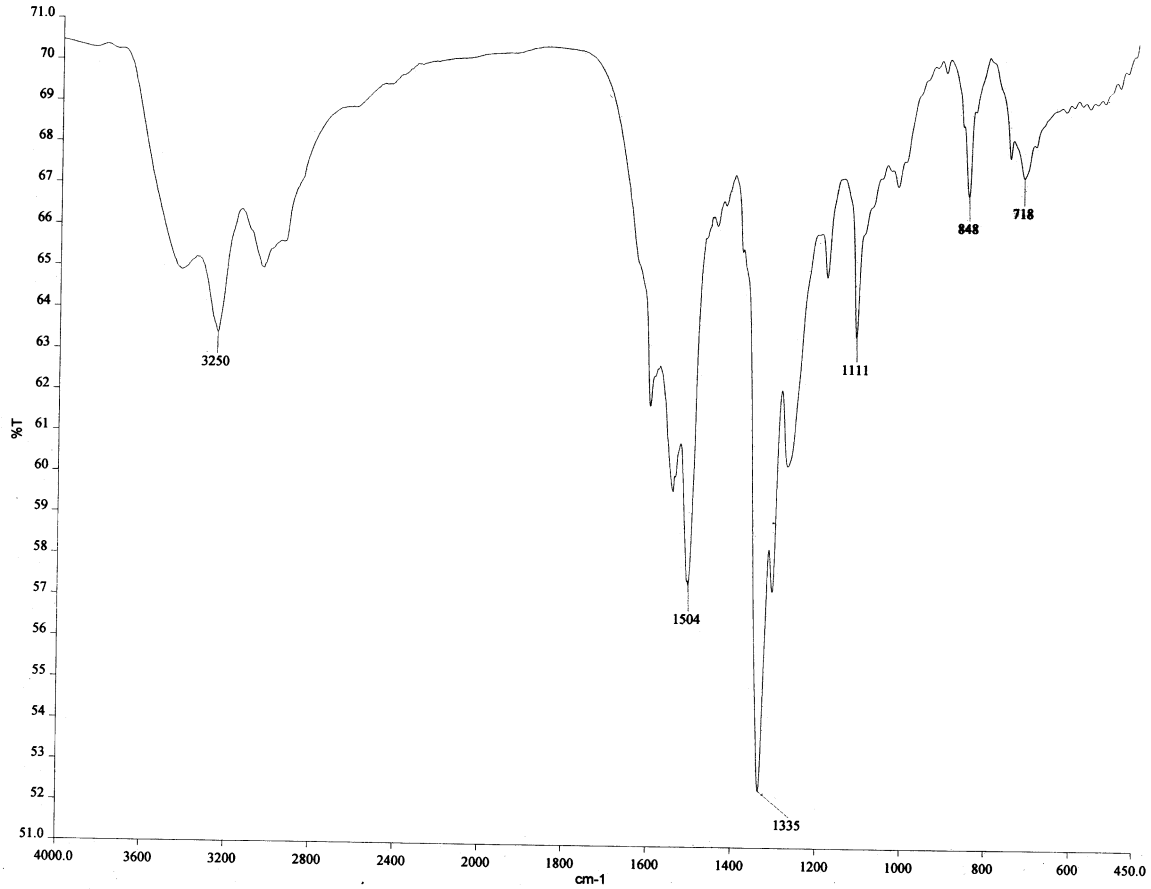

Figure S27. FT-IR spectrum of complex **5** recorded in KBr pellet.

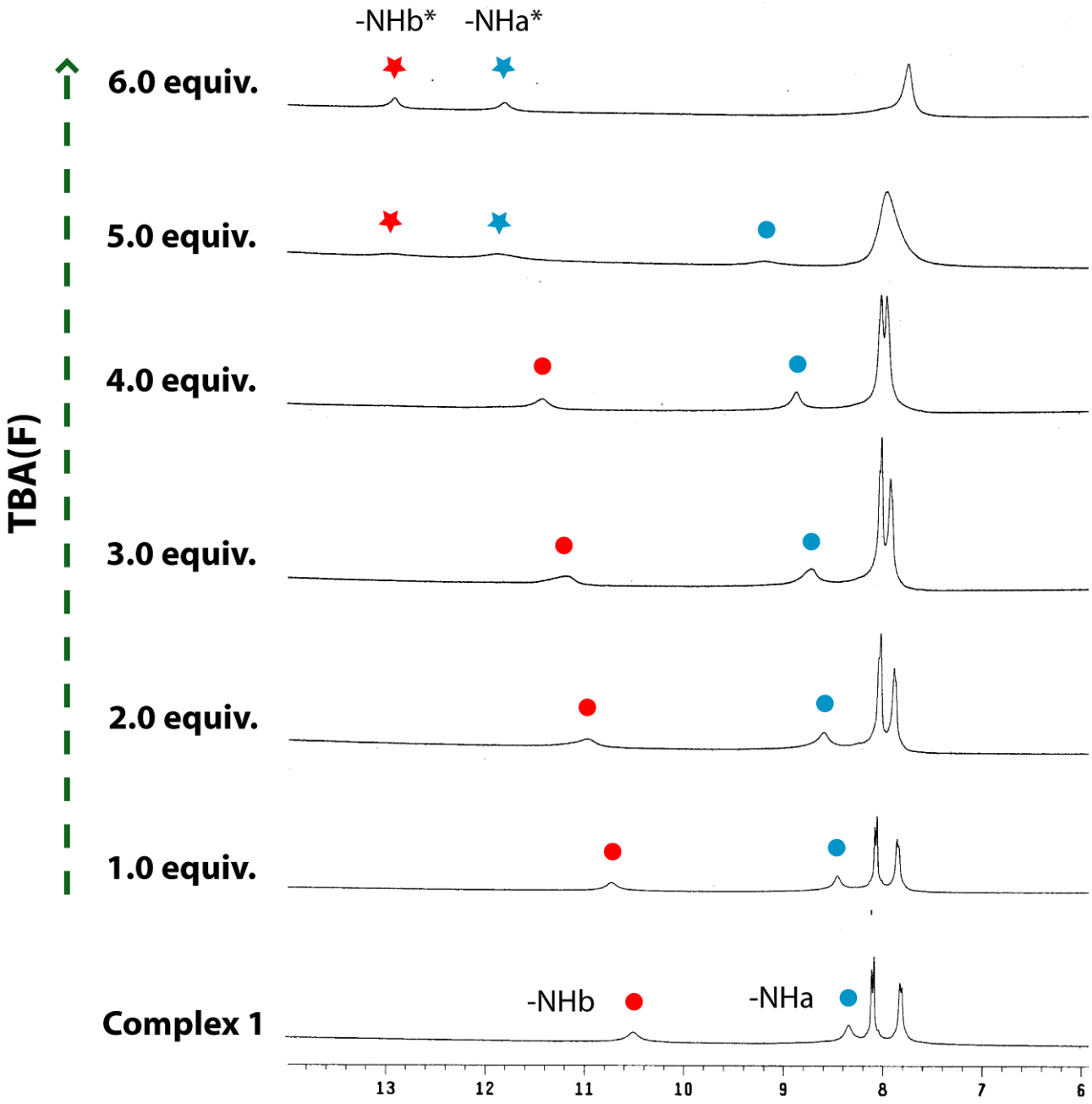

Figure S28. Expanded ^{1}H NMR spectra of **1a** obtained upon titration with increasing equivalents of TBAF in DMSO-d_6 showing the selective formation of phosphate capsule (**1**) in solution.

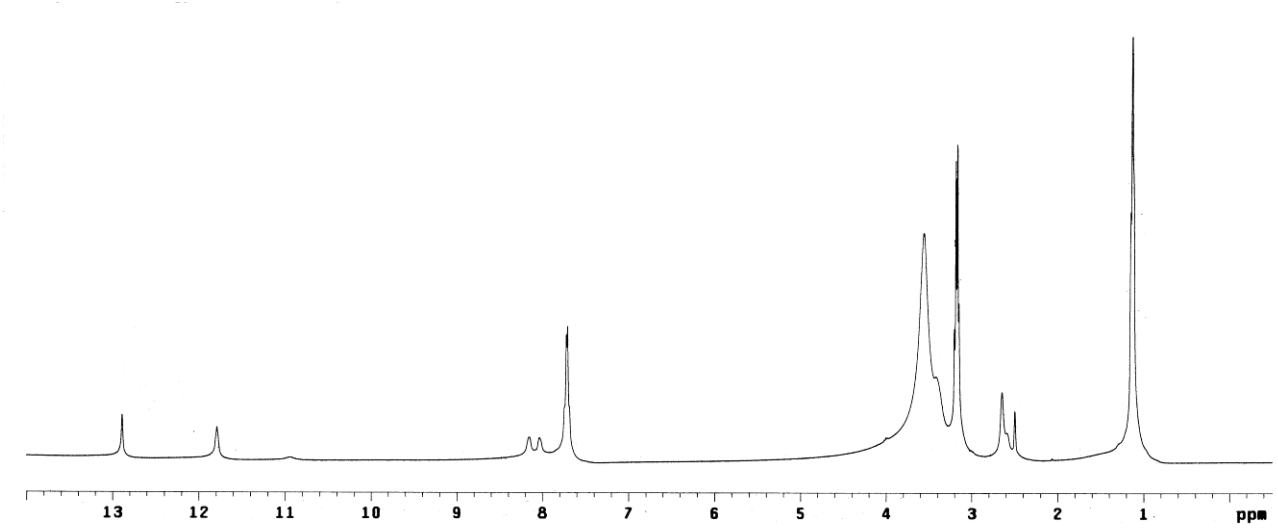

Figure S29. ^{1}H NMR spectrum of complex **1a** in presence of excess TEA(AcO) in DMSO-d_6 showing the selective formation of phosphate capsule (**1b**) in solution.

Additional Crystallographic data:

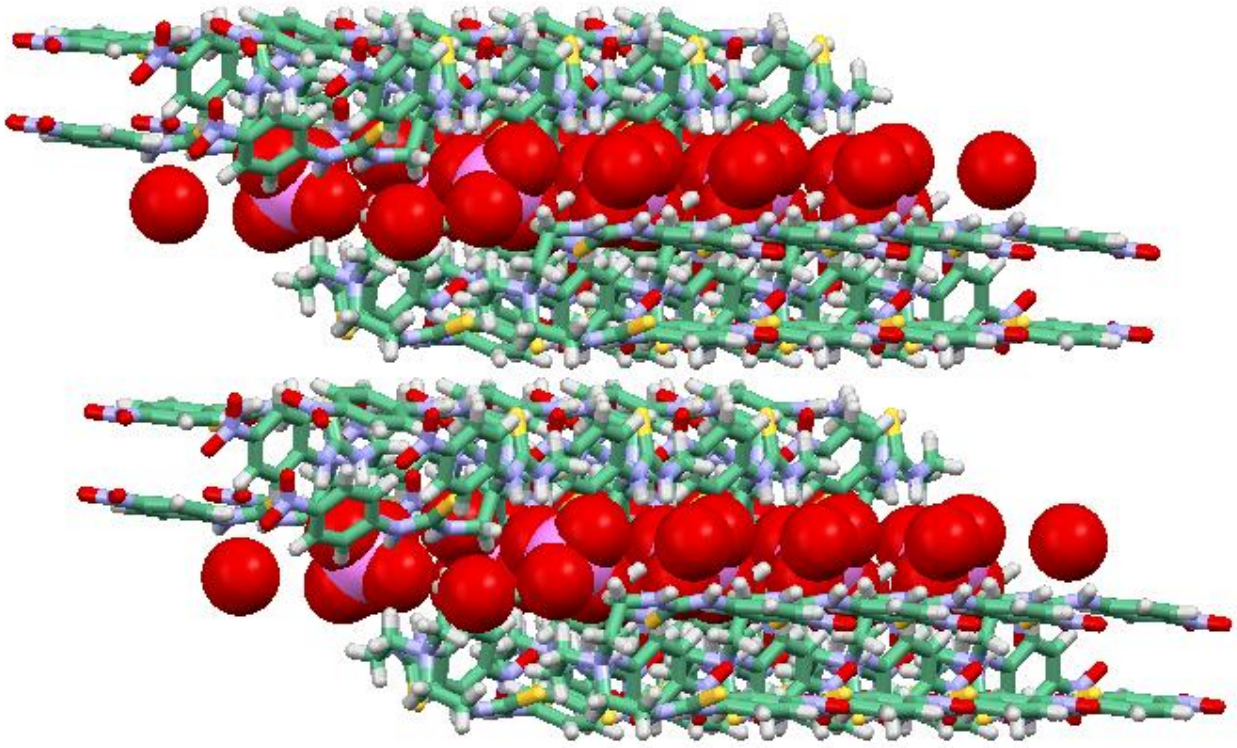

Figure 30. Crystal packing diagram of complex **1a** (view down the crystallographic c-axis).

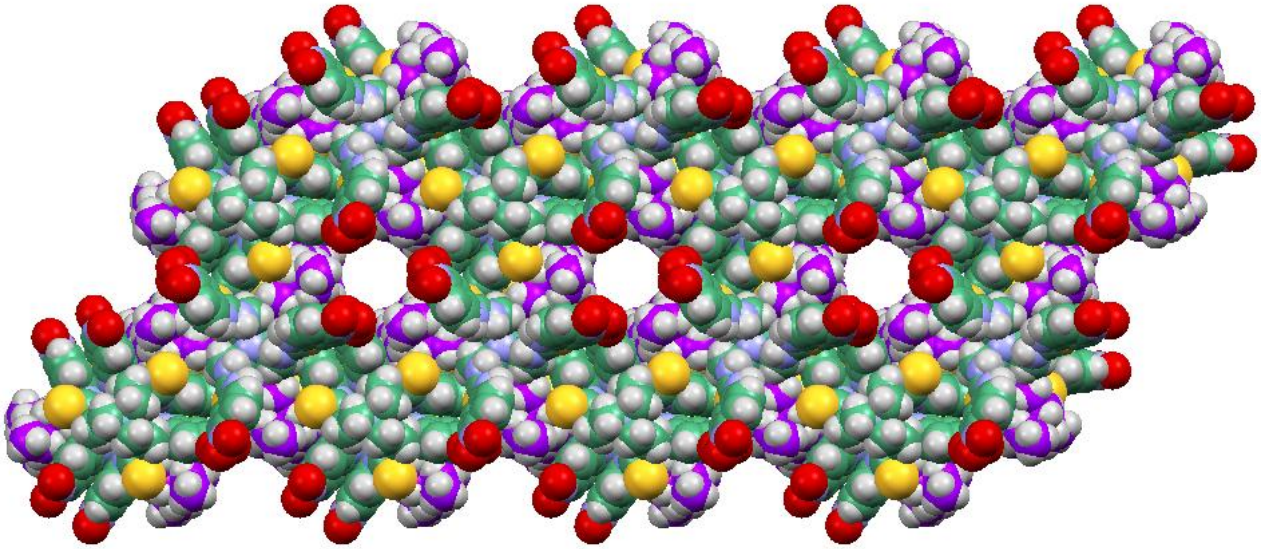

Figure 31. Crystal packing diagram of complex **1b**, showing the cylindrical voids of 568 Å^3 (view down the crystallographic c-axis).

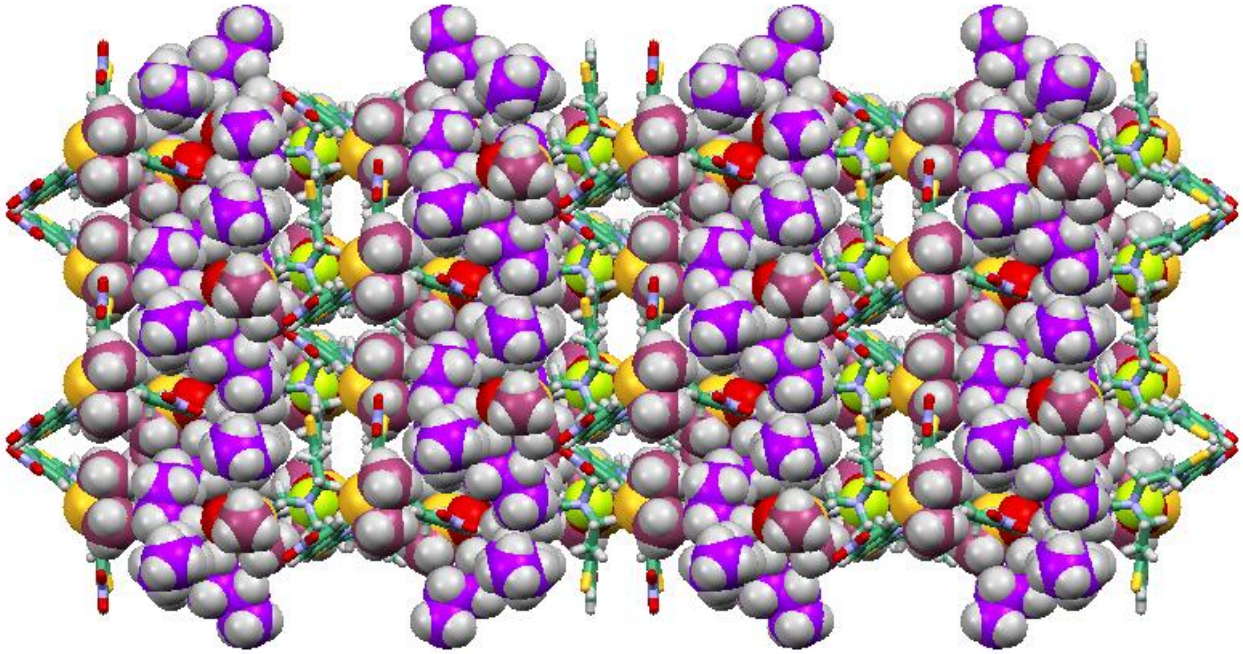

Figure 32. Crystal packing diagram of complex **2a** (view down the crystallographic c-axis).

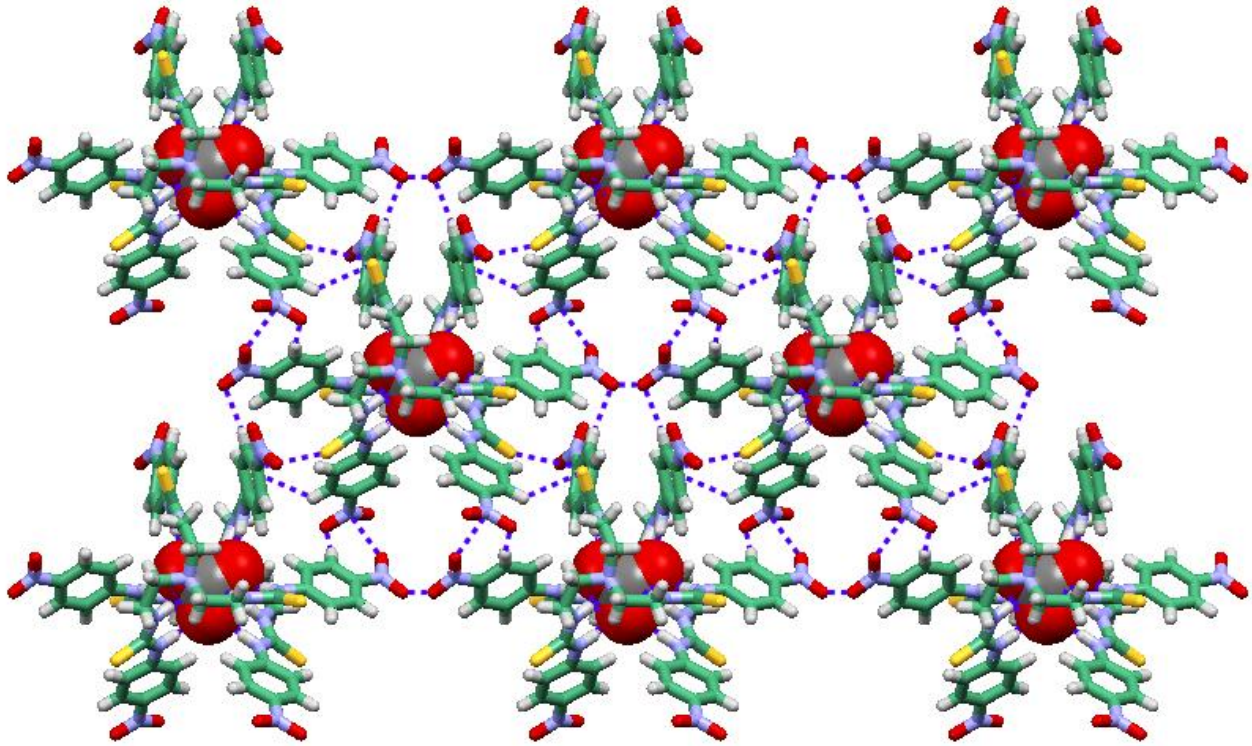

Figure 33. Crystal packing diagram of complex **3** (view down the crystallographic c-axis).

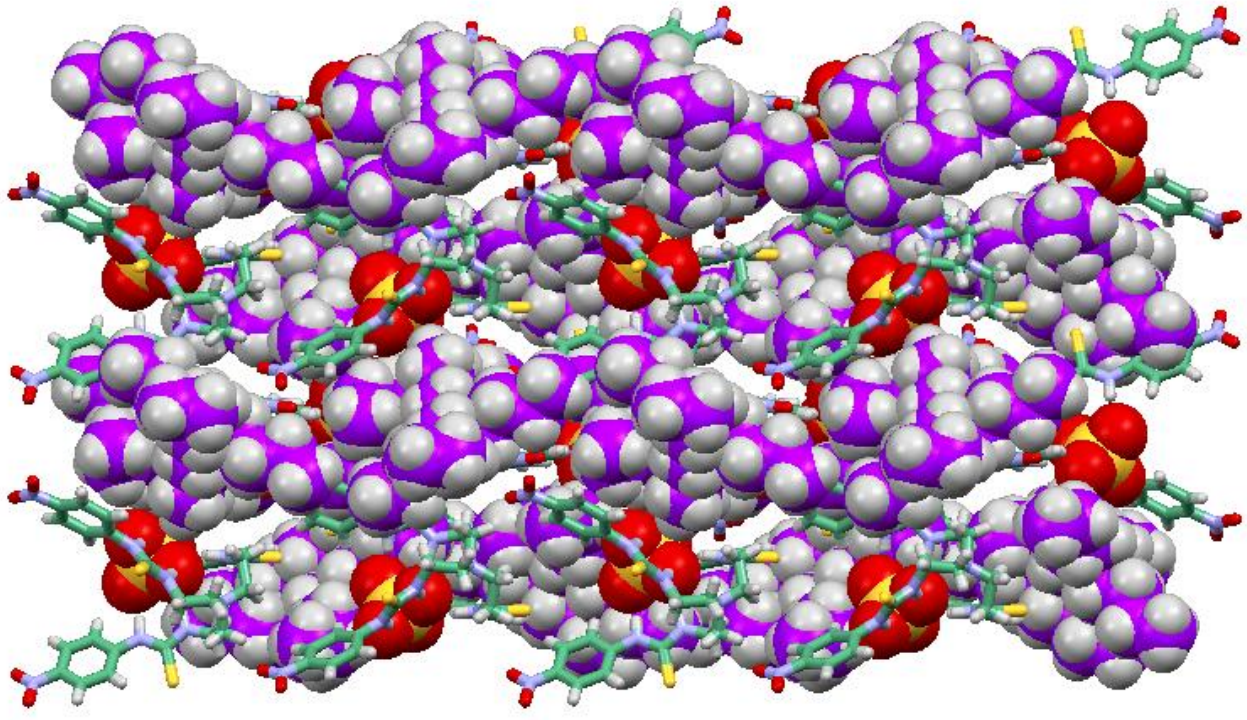

Figure 34. Crystal packing diagram of complex **4** (view down the crystallographic a-axis).

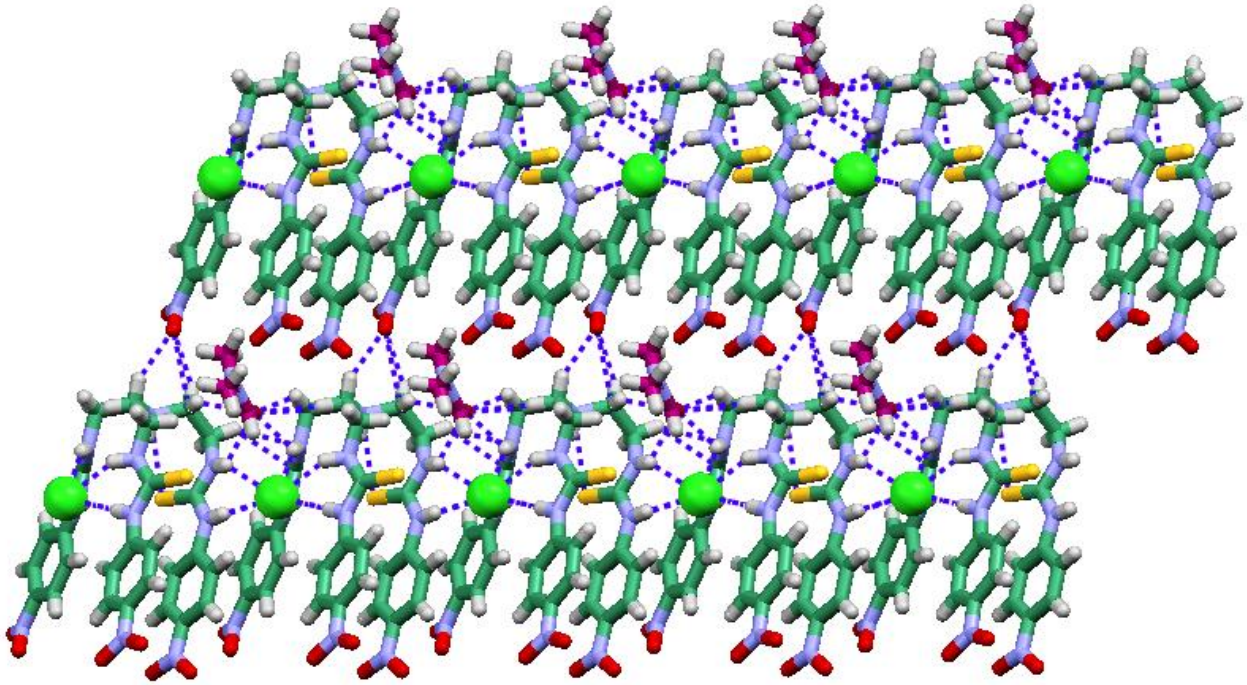

Figure 35. Crystal packing diagram of complex **5** (view down the crystallographic b-axis).